HHS Public Access

Author manuscript

Mucosal Immunol. Author manuscript; available in PMC 2023 October 23.

Published in final edited form as:

Mucosal Immunol. 2023 October ; 16(5): 699–710. doi:10.1016/j.mucimm.2023.07.004.

GL7 ligand expression defines a novel subset of CD4+ T_{RM} cells in lungs recovered from pneumococcus

Carolina Lyon De Ana[1,2], **Anukul T. Shenoy**[1,9], **Kimberly A. Barker**[1,2], **Emad I. Arafa**[1,3], **Neelou S. Etesami**[1,2], **Filiz T. Korkmaz**[1,4], **Alicia M. Soucy**[1], **Michael P. Breen**[1,2], **Ian M.C. Martin**[1], **Brian R. Tilton**[1], **Priyadharshini Devarajan**[4], **Nicholas A. Crossland**[6,7], **Riley M.F. Pihl**[1,3,5], **Wesley N. Goltry**[1], **Anna C. Belkina**[1,5,7], **Matthew R. Jones**[1,3], **Lee J. Quinton**[1,2,3,4,7], **Joseph P. Mizgerd**[1,2,3,8,✉]

[1]Pulmonary Center, Boston University Chobanian & Avedesian School of Medicine, Boston, Massachusetts, USA.

[2]Department of Virology, Immunology, & Microbiology, Boston University Chobanian & Avedesian School of Medicine, Boston, Massachusetts, USA.

[3]Department of Medicine, Boston University Chobanian & Avedesian School of Medicine, Boston, Massachusetts, USA.

[4]Department of Medicine, University of Massachusetts Chan Medical School, Worcester, Massachusetts, USA.

[5]Flow Cytometry Core Facility, Boston University Chobanian & Avedesian School of Medicine, Boston, Massachusetts, USA.

[6]National Emerging Infectious Diseases Laboratories, Boston University, Boston, Massachusetts, USA.

[7]Department of Pathology and Laboratory Medicine, Boston University Chobanian & Avedesian School of Medicine, Boston, Massachusetts, USA.

[8]Department of Biochemistry & Cell Biology, Boston University Chobanian & Avedesian School of Medicine, Boston, Massachusetts, USA.

[9]Department. of Microbiology and Immunology, University of Michigan Medical School, Ann Arbor, Michigan, USA.

✉ jmizgerd@bu.edu .

AUTHOR CONTRIBUTIONS

Conceptualization, CLDA and JPM; Methodology, CLDA and JPM; Investigation, CLDA, ATS, KAB, EIA, NSE, FTK, AMS, MPB, IMCM, BRT, RMFP, PD, NAC, and WNG; Validation, CLDA, ATS, RMFP and ACB; Supervision, CLDA and JPM; Project Management, CLDA; Software, CLDA, ACB; Formal Analysis, CLDA; Data Curation, CLDA; Visualization, CLDA and JPM; Resources, NAC, ACB, MRJ, LJQ and JPM;
Writing, CLDA; Review-Editing, CLDA, ATS, KAB, EIA, NSE, FTK, AMS, MPB, IMCM, BRT, PD, NAC, RMFP, WNG, ACB, MRJ, LJQ and JPM; Funding Acquisition, JPM.

DECLARATION OF COMPETING INTERESTS

The authors have no competing interests to declare.

APPENDIX A. SUPPLEMENTARY DATA

Supplementary data to this article can be found online at https://doi.org/10.1016/j.mucimm.2023.07.004.

Abstract

Streptococcus pneumoniae is the most common etiology of bacterial pneumonia, one of the leading causes of death in children and the elderly worldwide. During non-lethal infections with *S. pneumoniae*, lymphocytes accumulate in the lungs and protect against reinfection with serotype-mismatched strains. Cluster of differentiation $CD4^+$ resident memory T (T_{RM}) cells are known to be crucial for this protection, but the diversity of lung $CD4^+$ T_{RM} cells has yet to be fully delineated. We aimed to identify unique subsets and their contributions to lung immunity. After recovery from pneumococcal infections, we identified a distinct subset of $CD4^+$ T cells defined by the phenotype $CD11a^{hi}CD69^+GL7^+$ in mouse lungs. Phenotypic analyses for markers of lymphocyte memory and residence demonstrated that $GL7^+$ T cells are a subset of $CD4^+$ T_{RM} cells. Functional studies revealed that unlike $GL7^-$ T_{RM} subsets that were mostly (RAR-related Orphan Receptor gamma T) $ROR\gamma T^+$, $GL7^+$ T_{RM} cells exhibited higher levels of (T-box expressed in T cells) T-bet and Gata-3, corresponding with increased synthesis of interferon-γ, interleukin-13, and interleukin-5, inherent to both T helper 1 (T_H1) and T_H2 functions. Thus, we propose that these cells provide novel contributions during pneumococcal pneumonia, serving as important determinants of lung immunity.

INTRODUCTION

Lower respiratory infections impart one of the highest global burdens of disease worldwide and are a leading cause of death, especially in children and the elderly[1–3]. The most common bacterial source of pneumonia is *Streptococcus pneumoniae* (*Spn*). Over 100 different serotypes have been identified based on differences in the *Spn* capsule[4]. While effective serotype-specific vaccines have reduced mortality from invasive pneumococcal disease worldwide[5,6], infections with non-vaccine serotypes continue to increase[7,8]. Our group and others have demonstrated that self-limiting experimental pneumonia or immunization leads to an accumulation of resident memory lymphocytes that provide protection across multiple *Spn* serotypes, termed heterotypic immunity[9–11]. Leveraging our knowledge about these resident lymphocytes will be crucial in developing strain-independent *Spn* vaccines.

Resident memory T cells (T_{RM}) localize to non-lymphoid tissues and deliver local and fast effector functions at the time of reinfection[9–13]. Lung T_{RM} cells have been shown to provide crucial long-term protection against many bacterial and viral agents[10,12–15]. T_{RM} cells deliver essential cues to their environment and cooperate with epithelial cells, B cells, and other T cells to choreograph important functions needed for immune protection, such as lymphocyte and neutrophil recruitment[16–18]. T_{RM} cells have been characterized by expression of the surface markers cluster of differentiation CD11a and CD69 at rest[10,12], although heterogeneity within this population is gaining recognition[18,19]. Previous work by our group demonstrates the presence of diverse and novel subsets of $CD4^+$ and $CD8^+$ T_{RM} and B resident memory cells in mouse lungs after pneumococcal exposures[20,21], but the extent of lung T_{RM} cell diversity and their roles in immune protection are still unclear.

In this work, we used full-spectrum flow cytometry (FSFC) to study $CD4^+$ T cells in the lungs of *Spn*-experienced mice. We have identified previously undescribed subsets of

CD4$^+$ T_{RM} cells that express the GL7 antibody ligand, known as a marker of germinal center B cells. GL7 is a monoclonal antibody that recognizes surface glycans sialylated with N-Acetylneuraminic Acid (Neu5Ac)[22]. Throughout this study, we will denote cells expressing the ligand of GL7 (Neu5Ac) as GL7$^+$. Our analyses revealed that this novel subset of GL7$^+$ T cells represents a non-recirculating resident population of CD4$^+$ T_{RM} cells with a unique transcription factor profile that secretes a distinct combination of cytokines. Our study introduces GL7$^+$ T_{RM} cells as a discrete population of lung-resident lymphocytes arising after recovery from pneumococcal pneumonia.

RESULTS

Recovery from pneumonia leads to subpopulations of CD4$^+$ T cells arising in the lungs

CD4$^+$ T cells mediate heterotypic immune protection against pneumococcal pneumonia[10,16]. Comprehensive phenotyping of *Spn*-experienced lungs revealed a previously unappreciated heterogeneity of resident lymphocytes[20]. Following this approach, we combined FSFC using a 22-color immunopheno-typing panel[20] to further investigate lung CD4$^+$ T_{RM} cells in *Spn*-experienced lungs. Adult mice received two intratracheal (i.t.) instillations of *Spn* serotype 19F (Sp19F) directed to the left lobes (LLs) (Fig. 1A). The two infections result in a self-limiting pneumonia that promotes heterotypic immune remodeling[10]. After a resting period of 30 days, we collected the lungs and processed them for further studies. We used a panel of 21 surface markers to characterize and distinguish lymphocyte subsets[20], concatenated data from six experienced mice, subsetted live extravascular (i.v.CD45.2$^-$) CD4$^+$ T cells (Supplementary Fig. 1), and projected the multiparameter data into 2-dimensional space using optimized parameter T-distributed stochastic neighborhood embedding (opt-SNE)[23] (Fig. 1B). To identify the cells subsets on the resulting map, we overlaid heatmaps of normalized expression of each marker over the opt-SNE visualization (Fig. 1C, Supplementary Fig. 1B). We observed that three markers, CD11a, CD69, and GL7, could separate CD4$^+$ T cells into distinct populations. Following heatmap expression, we designed a supervised gating strategy to categorize lung CD4$^+$ T cells which confirmed four major subsets: CD11a^{hi}CD69$^+$GL7$^-$, CD11a^{hi}CD69$^+$GL7$^+$, CD11a^{hi}CD69$^-$GL7$^-$ and CD11a^{lo} (Figs. 1D and 1E, Supplementary Fig. 2A), referred to henceforth as CD69$^+$GL7$^-$, CD69$^+$GL7$^+$, CD69$^-$GL7$^-$ and CD11a^{lo} respectively. All but the CD11a^{lo} subsets were CD44^{hi} and CD62L^{lo}, characteristic of memory T cells, while the CD11a^{lo} cells were CD44^{lo}CD62L^{hi}, characteristic of naive T cells[24,25] (Figs. 1F and 1G). These phenotypes suggest that both CD69$^+$ populations were T_{RM} cells[12–14], with expression of GL7 ligand differentiating a distinct subset (Figs. 1F and 1G). The GL7-reactive CD4$^+$ cells were observed in loose aggregates within the interstitial connective tissue of bronchovascular bundles after recovery from pneumococcal pneumonia, in association with other CD4$^+$ cells that were not GL7-reactive (Fig. 1H).

GL7 detects surface glycans sialylated with Neu5Ac[22,26]. In resting lymphocytes, the enzyme cytidine monophospho-Neu5Ac hydroxylase (CMAH) catalyzes the hydroxylation of Neu5Ac into N-glycolylneuraminic acid (Neu5Gc)[26]. During lymphocyte activation, *Cmah* is downregulated, resulting in glycan sialylation with Neu5Ac[22,26–29]. GL7 ligand expression occurs in germinal center B cells (B_{GC}) and GC T follicular helper (T_{FH})

cells, but such phenotype has not been reported in memory T cells[28,30]. To examine if $CD69^+GL7^+$ cells have a reduced level of CMAH, we measured *Cmah* transcripts in $CD69^+GL7^+$ and $CD69^+GL7^-$ cells sorted from experienced mouse lungs. $CD69^+$-$GL7^+$ cells demonstrated a reduced level of *Cmah* transcripts, suggesting the expression of GL7 ligand associates with a reduced level of the enzyme and an additional phenotypic difference between T_{RM} cell subsets (Fig. 1I, Supplementary Fig. 2B). Together, these results suggest $CD4^+$ T_{RM} cells in pneumococcal experienced mouse lungs can be separated into subpopulations based on their differential expression of surface markers including the GL7 ligand Neu5Ac.

The $GL7^+$ T cells in recovered lungs are not circulating, proliferating, follicular, or restricted to pneumococcal infections

In agreement with previous reports by our group and others[10,11,16,21], we observe that all four subsets of lung T cells, $CD11a^{hi}CD69^+GL7^-$, $CD11a^{hi}CD69^+GL7^+$, $CD11a^{hi}CD69^-GL7^-$ and $CD11a^{lo}$, increased in number after pneumococcal experience (Fig. 2A). The largest fraction of $CD4^+$ T cells in naïve lungs corresponded to $CD11a^{lo}$ cells; in experienced lungs, $CD11a^{hi}$ subsets predominated, including the more resident-like $CD69^+$-$GL7^-$ (Fig. 2A), supporting immune remodeling after infection. To further understand the dynamics of these subsets after *Spn* infections, we collected the left lung lobes at eight different timepoints from 0 to 35 days after exposure (Fig. 2B). The second Sp19F infection, designed to facilitate local antigen presentation in the lung, triggered acute accumulation of T cells (Supplementary Fig. 3A). The numbers of cells from all four subsets reached a maximum at 3 days after the second infection (10 dpi) (Fig. 2C). From 24 to 35 dpi both $CD69^+GL7^+$ and $CD69^+GL7^-$ subsets plateau and their cell numbers stabilized, while $CD69^-$ and $CD11a^{lo}$ cells continuously decreased over these timepoints (Fig. 2C). The proportion of $CD4^+$ T cells that are $CD69^+GL7^+$ increased in the lungs after the second infection, and it became progressively greater over successive timepoints (Fig. 2D, Supplementary Fig. 3A).

T_{RM} cells reside in the lung after infections rather than regularly recirculating through blood and secondary lymphoid organs[10–15]. To evaluate if the $CD69^+GL7^+$ and $CD69^+GL7^-$ subsets were extravasating from the lungs, we treated experienced mice with FTY720 every alternate day for 12 days prior to lung collection (Supplementary Figs. 3B and 3C). FTY720 prevents sphingosine-1-phosphate (S1P)-mediated T cell egress from lymph nodes and has been widely utilized to evaluate T cell migration in multiple tissues[31–33]. We observed the proportion of neither $CD69^+GL7^+$ nor $CD69^+GL7^-$ subsets of $CD4^+$ T cells were affected by FTY720 treatment, while $CD11a^{lo}$ subsets were reduced significantly (Figs. 2E and 2F). These data suggest that the $GL7^+$ subset, like other T_{RM} cells[31–33], are not in constant S1P-mediated circulation but instead, get retained in the lungs long-term.

To determine whether $CD69^+GL7^+$ cells that accumulated in *Spn*-experienced lungs were in a state of proliferation, we measured their expression of Ki67[19]. Although $Ki67^+$ cycling cells were abundant in the first days after infection, both $CD69^+GL7^+$ and $CD69^+GL7^-$ subsets were equally low in Ki67 expression at the late timepoints (Fig. 3A, Supplementary Fig. 4A). Thus, neither of the two T_{RM} cell subsets were proliferating in the resting lungs.

Despite the absence of actively proliferating cells, these $GL7^+$ subsets of memory $CD4^+$ T cells could persist in the lungs for at least 6 months (Figs. 3B and 3C, Supplementary Fig. 5B). Together, these data suggest $CD69^+GL7^+$ T cells in the *Spn*-experienced lung have resident memory-like characteristics resembling T_{RM} cells[19]. Hereafter, $CD69^+GL7^+$ and $CD69^+GL7^-$-subsets from these lungs will be referred to as $GL7^+$ and $GL7^-$ T_{RM} cells.

GL7 ligand can be expressed on T_{FH} cells in germinal centers[28,30]. A subset of lung-resident cells with T_{FH}-like biology, T resident helper[7] cells, arises in the lungs of mice recovered from influenza infection[17,18]. Influenza infections as well as *Klebsiella pneumoniae* preparations elicit tertiary lymphoid structures in the lungs[34–36], which are not observed after recovery from pneumococcus[10,11]. Although the numbers of CD4+ TRM cells varied across microbial challenges, $CD69^+GL7^+$ memory $CD4^+$ cells were identified in all settings and at similar proportions (Figs. 4C and 4D). To evaluate if the $GL7^+$ T_{RM} cells in lungs recovered from pneumococcus resemble T_{RH} cells that have been described after influenza, we evaluated the expression of T_{RH}-associated markers[17,18]. Using a mechanical digestion method reported to conserve T_{RH} cell recovery from the lungs[17,18], we observed very few $PSGL1^{low}FR4^{high}$ T_{RH} cells (Fig. 3G, Supplementary Fig. 5A). $GL7^+$ cells were found among the $PSGL1^{high}$-$FR4^{low}$ T_{RM} cells, not the $PSGL1^{low}FR4^{high}$ T_{RH} cells (Figs. 3H and 3J, Supplementary Fig. 5A). Furthermore, $BCL6^+$ and $CXCR5^+$ cells were rare among the memory $CD4^+$ T cells in lungs from mice recovered from pneumococcus, and when found these cells tended to be $GL7^-$ (Supplementary Fig. 5B). We conclude that $GL7^+$ T_{RM} cells are distinct from follicular-like lung T_{RH} cells.

Cytokine expression by $GL7^+$ T_{RM} subsets reveals functional diversity

A cardinal function of T_{RM} cells in mucosal tissues is cytokine secretion[10,12,14,15,37]. Our group and others have shown that cytokines secreted by lung $CD4^+$ T_{RM} cells provide important signals to neighboring cells to orchestrate immune protection[16–18,21]. To determine if GL7 expression highlighted a functionally distinct subset of lung $CD4^+$ T cells, we designed an FSFC panel that included four cytokines and major T_{RM} lineage markers. We combined intracellular cytokine staining (ICS) with preliminary antibody labeling to track GL7 and CD69 surface marker expression throughout *ex vivo* stimuli with PMA/Ionomycin. As expected, the majority of lung $CD4^+$ T cells from *Spn*-recovered lungs expressed IL-17A upon stimulation, and this applied to both the $GL7^+$ and $GL7^-$ subsets (Fig. 4A, Supplementary Fig. 6A). However, the distribution of cytokine-secreting cells differed between the T cell subsets. Compared to $GL7^-$ T_{RM} cells from the same lung, the $GL7^+$ T_{RM} cells were less frequently IL-17A-producers, and more frequently IFN-γ or IL-5 and/or IL-13 producers (Figs. 4A–4C). This insinuates a potential functional difference in this subset of T cells, less T_H17-like and more prone to T_H1 and T_H2-like responses. These data suggest $GL7^+$ T_{RM} cells have a functional difference that results in a reduced output of IL-17A and an increase in IFN-γ, IL-5, and/or IL-13 after stimulation.

$GL7^+$ T_{RM} subsets have distinct transcription factor profiles

Cytokine expression from helper T cells is typically dependent on cellular phenotypes dictated by lineage-defining transcription factors (LDTF)[38]. We used a flow cytometry panel with T-bet, Gata-3, RORγT, and FoxP3, to help us discriminate the T_H1, T_H2, and T_H17

helper and T_{reg} subsets of T cells, respectively[21,38]. Within the GL7$^+$ T_{RM} subset, there was a lower frequency of RORγT$^+$ and more Gata-3$^+$ cells in comparison to the GL7$^-$ counterparts (Figs. 5A and 5B, Supplementary Fig. 7A). FOXP3$^+$ cells were rare among both GL7$^+$ and GL7$^-$ T_{RM} cells, but a little less so in the former (Supplementary Fig. 7B) This implies that the GL7$^+$ T cells may be more predisposed to the T_H2-like lineage and less predisposed to the T_H17-like lineage compared to the GL7$^-$ cells from the same lungs, consistent with the cytokine expression data.

While expression of a single transcription factor has been widely used to define T_H cell lineages[38], multi-lineage CD4$^+$ T cell plasticity is known[21,39,40]. Studies by our group recently demonstrated that many T_{RM} cells in *Spn*-experienced lungs express multiple lineage-defining transcription factors simultaneously[20,21]. To evaluate if GL7$^+$ T_{RM} cells represented a subset with unique combinations of transcription factors, we combined LDTF data from Fig. 4 with a nested manual gating strategy that measured the expression of one, two, or three of the factors simultaneously in each T_{RM} subset among FOXP3$^-$ cells (Supplementary Fig. 7C)[21]. While cytokine analyses suggested that multifunctionality was rare (Supplementary Fig. 6B), lung T cells often exhibited multiple lineage-defining transcription factors (Fig. 5D) and the relative multipotency index[21] revealed that the GL7$^+$ T_{RM} cells tend to express fewer compared to the GL7$^-$ counterparts (Fig. 5C). Examining the co-expression phenotypes more specifically, we identified eight subpopulations, each of which was present in both T_{RM} subsets. The most common phenotype was Gata-3$^+$RORγT$^+$ cells, which may reflect a skewing toward Th2/Th17 (Fig. 5D). Within GL7$^-$ T_{RM} cells, the second most common subtype was a triple-negative population that did not express any of the lineage-defining transcription factors included in our study. In GL7$^+$ T_{RM} cells, the second most common subtype was Gata-3$^+$ cells lacking the other transcription factors, which were significantly less abundant within the GL7$^-$ population (Fig. 5D, Supplementary Fig. 6B).

These data further support the concept that GL7$^+$ cells represent a distinct subphenotype of lung T_{RM} cells. While subsets exist among both GL7$^+$ and GL7$^-$ T_{RM} cells, the differences in distribution suggest the former tilt away from T_H17 and toward T_H2 compared to the latter, consistent across transcription factor content and cytokine expression.

Upon further evaluation, we observed different levels of expression of GL7 within GL7+ T_{RM} cells, which we defined as GL7^{hi} and GL7^{lo}. Inspection of the GL7 *vs.* transcription factor data suggested that cells with lower or higher amounts of GL7 (Fig. 6A) may have different expression levels of LDTFs. The GL7^{lo} subsets had frequencies of RORγT$^+$ cells and T-bet$^+$ cells that matched GL7$^-$ T_{RM} cells, but Gata-3$^+$ cells were enriched in GL7^{lo} T cells (Fig. 6B–C). In contrast, the GL7^{hi} subsets had decreased frequencies of RORγT$^+$ cells and increased frequencies of T-bet$^+$ cells compared to the GL7$^-$ counterparts, while Gata-3$^+$ cells were unchanged (Fig. 6B–C). Altogether, these transcription factor results match the cytokine expression data well, providing consistent evidence for decreased T_H17 but increased T_H1 and T_H2 skewing in the GL7$^+$ lung CD4$^+$ T_{RM} cells compared to the GL7$^-$ lung CD4+ T_{RM} cells.

DISCUSSION

Our study highlights a novel population of resting $CD4^+$ T cells residing in lungs that have recovered from pneumonia, distinguished by expression of Neu5Ac that is recognized by the GL7 monoclonal antibody. These cells share many characteristics with $GL7^-$ T cells from these lungs, including a stable and long-lived $CD11a^{Hi}CD69^+CD62L^{Lo}CD44^{Hi}Ki67^-$ phenotype, which led us to conclude they are lung-resident memory lymphocytes, further supported by FTY720 studies. However, the $GL7^+$ T cells in these lungs differ from their $GL7^-$ neighbors. The former expresses lower levels of the CMAH enzyme contain a different balance of LDTFs at rest and produce a different mixture of cytokines when activated. We propose that GL7 marks a previously unrecognized subset of lung T_{RM} cells.

GL7 reactivity is not unprecedented for mouse lymphocytes. GL7 ligand expression has been detailed in cells from mice in primary and secondary lymphoid organs, including B_{GC} cells[22,26,27,41] as well as a subset of T_{FH} cells whose surface markers include $CD4^+CXCR5^{Hi}GL7^+$[28,30]. While $CXCR5^+$ and $BCL6^+$ memory $CD4^+$ T cells could be recovered from *Spn*-experienced lungs using manual digestion methods, they were mostly $GL7^-$. The $GL7^+$ subsets also did not express markers associated with the TFH-like lung T_{RH} cells[17,18], suggesting that these $GL7^+$ T_{RM} may not be the T_{FH} phenotype or the newly reported and related T_{RH} cells[17,18]. GL7 ligand expression is acutely upregulated on B cells and T cells due to *in vitro* stimulation[22,26,27,29]. The $GL7^+$ phenotype in these activated naïve cells is due to a transient decrease in CMAH, the reduction of which results in the surface glycan sialylation with Neu5Ac[27,29].

We demonstrate that $GL7^+$ T_{RM} cells have low CMAH-like activated naïve cells but with several important distinctions: 1) they are found in resting lungs that have recovered from bacterial or viral pneumonia, but without any ongoing infection or inflammation; 2) they exhibit markers of resident memory cells, 3) they form a stable population that persists long-term; 4) they do not circulate out of the lungs; 5) and they are not proliferating. We believe this may be the first evidence for GL7 ligand expression on resting or memory T cells.

We postulate that $GL7^+$ cells are a distinct subset of lung CD4 + T_{RM} cells that may influence the immune tone of lungs responding to a heterotypic respiratory infection. Most memory T_{RM} cells after a *Spn* lung infection are of the T_H17 lineage that predominantly secretes IL-17A during activation or subsequent reinfection[10,21]. Previous work from our group and others revealed T_{RM} cells that expressed transcription factors from multiple lineages and could secrete diverse cytokines after *ex vivo* stimulation[20,35,42]. Our current work supports these claims and shows such plasticity applies to both $GL7^-$ and $GL7^+$ subsets of T_{RM} cells. However, the $GL7^+$ subset appears to favor T_H1 and T_H2 phenotypes more and the T_H17 phenotype less, in comparison to the more numerous $GL7^-$ lung T_{RM} cells. This conclusion is based on balances of both the transcription factors and the cytokines in these cells; and suggests T_{RM} cells in *Spn*-recovered lungs share many similarities, but the $GL7^+$ subset is more poised to provide T_H1 and T_H2 responses than are $GL7^-$ T_{RM} cells, which more robustly favor T_H17 responses.

There is still much to learn about these $CD4^+$ T_{RM} cell subsets, but these first results suggest a possible model related to T cell contributions to immune resistance and tissue resilience in acutely infected lungs that have a relevant heterotypic infection history[3,43]. T_H17 responses are key to many aspects of immune resistance against extracellular microbes like pneumococcus[34,44]; T_H1 responses foster antimicrobial activity against intracellular organisms, and also instruct the local immune remodeling of phagocytes and possibly other lung cells[45]; T_H2 responses promote tissue repair and regeneration after injury[42,46]. Thus, it is possible that the more numerous $GL7^-$ T_{RM} cells are most critical to the immune resistance and the elimination of pneumococcus from acutely infected lungs[10,16], whereas the scarcer $GL7^+$ T_{RM} cells affect immunomodulation and repair during the tissue recovery stage after pneumonia.

Humans have an inactive *CMAH* gene and lack a functional CMAH enzyme, therefore surface glycans on human lymphocytes are uniformly sialylated with Neu5Ac[47,48]. Human lung T_{RM} cells therefore should not exhibit the surface sialylation variations seen here in mouse lung T_{RM} cells. However, humans use a different pathway that functions analogously to sialylation in mice. Humans differentially sulfate lymphocyte surface glycans, and the sulfation state toggles CD22 activation in human cells like glycan sialylation toggles CD22 in mouse lymphocytes[47–50]. CD22 interaction with Neu5Gc or sulfated Neu5Ac inhibits B cells[49]. A separation of T_{RM} cells by CD22 ligand expression may create subsets of cells that distinctly interact with and regulate $CD22^+$ B cells, advancing another potential biological significance for these lung CD4+ T_{RM} cell subsets. The present results raise new questions about whether human lungs contain two CD4+ T_{RM} cell subpopulations which differ in Neu5Ac sulfation.

As the roles of $CD4^+$ T_{RM} cells in lung immunity continue to be elucidated, we begin to understand that T_{RM} cells are a diverse community with myriad functions that contribute to lung protection. We propose $GL7^+$ T_{RM} cells as one such subset, whose functions may involve differential cytokine secretion, contributing to the overall immune roles of lung T_{RM} cells. Future efforts to develop mucosal vaccines that trigger a robust immune environment in the lungs should consider how the diverse subsets of resident lymphocytes provide mechanisms of protection that result in more effective elimination of microbes and better protection of tissues against damage.

METHODS

Mice

We obtained 6-week-old C57BL/6J[51 000664] mice from The Jackson Laboratory (Bar Harbor, ME, USA). All mice were housed in specific pathogen-free conditions with a 12-hour light-dark cycle, and *ad libitum* access to standard chow and water. Then, 7–8-week-old mice that were adequately rested for 1 week after transfer were used for experiments. Mice were euthanized using isoflurane overdose and death was confirmed using pneumothorax before organ collections. Animal procedures were approved by Institutional Animal Care and Use Committee of Boston University (IACUC).

Streptococcus pneumoniae infections

Spn-specific lung-resident adaptive immunity was generated as previously described[10,12,13,15,37]. Mice were anesthetized with intraperitoneal (i.p.) administration of ketamine (50mg/kg) and xylazine (5mg/kg) before infection. After surgical exposure of the trachea, sterile saline, or *Spn* was administered intratracheally via a 24-gauge angiocatheter directed to the LL. Mice received 50μL saline containing 1–5 × 10^6 CFU of serotype 19F *Spn* (Strain EF3030) or saline. Seven days later, mice were exposed again to either saline or Sp19F and then allowed to recover for 28–35 days.

Influenza A infection

Mice were anesthetized with i.p. administration of ketamine (50mg/kg) and xylazine (5mg/kg) before infection. After surgical exposure of the trachea, Influenza A/PR8/34 (IAV) was administered intratracheally via a 24-gauge angiocatheter directed to the LL. Mice received 50μL saline containing ~15 plaque-forming units per mouse and allowed to recover for 40 days.

Heat-killed *Klebsiella pneumoniae* exposure

Klebsiella pneumoniae (KPN) ATCC strain 43816, serotype 2, was prepared as previously described[35]. It was expanded overnight at 37°C, 5% CO_2 in blood agar plates, and replated for 4 hours to reach log phase. Bacteria were diluted to 0.3 optical density measured at 600 nM, pelleted, and washed twice in sterile phosphate buffered saline (PBS) before resuspension in same. Bacteria were heat-killed by incubating at 70°C for 2 hours, and cultures confirmed no remaining bacterial viability. Mice were anesthetized with i.p. administration of ketamine (50mg/kg) and xylazine (5mg/kg). After surgical exposure of the trachea, heat-killed KPN was administered intratracheally via a 24-gauge angiocatheter directed to the LL. Mice received 50 uL containing 2.8 × 10^6 CFU-equivalents of heat-killed KPN. Seven days later, mice were re-exposed via similar heat-killed KPN administration, and then allowed to recover for 40 days.

Enzymatic digestion of mouse lungs for flow cytometry

To allow enumeration of extravascular (tissue) versus intravascular (circulating) fraction of lymphocytes, mice were anesthetized with i.p. administration of ketamine (50mg/kg) and xylazine (5mg/kg). Three minutes prior to euthanasia, 2 μg fluorochrome-labeled anti-CD45.2 antibody in 100 μL saline were retro-orbitally administered. Right and left lobes of lungs were collected separately in RPMI 1640 with 10% FBS before processing for flow cytometry. Lungs were digested in type 2 collagenase (Worthington Biochemicals, Lakewood, NJ, USA), DNase I (Sigma-Aldrich, St. Louis, MO, USA) and 2.5 mM CaCl2 in PBS for 1 hour at 250–300 rpm at 37°C. Digested lungs were filtered through a 70 μm cell strainer, followed by RBC lysis (Sigma-Aldrich, St. Louis, MO, USA). Cells were blocked with TruStain αCD16/CD32 Fc-Block (BioLegend, San Diego, CA, USA) before staining with optimized dilutions of antibodies (Supplementary Table 1) in 100 uL of FACS buffer and Brilliant Violet Buffer (BD Biosciences, Franklin Lakes, NJ, USA). Conventional flow cytometry was performed on LSR II Flow Cytometer (BD Biosciences, Franklin Lakes, NJ, USA). High-dimensional full-spectrum flow cytometry was performed on Cytek

Aurora (Cytek). SpectraFlo (Cytek) software was utilized for spectral unmixing of the raw full-spectrum data and unmixed data were analyzed with FlowJo software v10.7 (BD Biosciences, Franklin Lakes, NJ, USA). Gating strategies are provided in the Supplemental figures and were based on use of Fluorescence minus one (FMO) controls. For spectral unmixing and conventional compensation, UltraComp compensation beads (Thermo Fisher, Waltham, MA, USA) were used for all fluorochromes except when indicated. Total cell numbers were measured by multiplying the percentage fraction of specified leukocyte subset (in percentage of total) with the total number of cells recovered from each mouse lung.

Manual digestion of mouse lungs for flow cytometry

Experienced mice were anesthetized with i.p. administration of ketamine (50 mg/kg) and xylazine (5 mg/kg). Thirty minutes prior to euthanasia, 2.5 μg of Treg-protector™ anti-ARTC2 Nanobody (Biolegend, San Diego, CA, USA) was retro-orbitally administered administered. Then, 3–5 minutes prior to euthanasia, 2 μg fluorochrome-labeled anti-CD45.2 antibody in 100 μL saline were retro-orbitally administered. Right and left lobes of lungs were collected separately in cold PBS and manually filtered through a 70 μm cell strainer followed by RBC lysis with Ammonium-Chloride-Potassium (ACK) lysis buffer (Thermo Fisher, Waltham, MA, USA). Cells were blocked with TruStain αCD16/CD32 Fc-Block (BioLegend, San Diego, CA, USA) before staining with optimized dilutions of antibodies (Supplementary Table 1) in 100 uL of FACS buffer and Brilliant Violet Buffer (BD Biosciences, Franklin Lakes, NJ, USA).

Heterotypic immune timeline infection

Adult mice were anesthetized via i.p injection of ketamine and xylazine before infection. *Spn* suspended in sterile saline was instilled via a 24-gauge angiocatheter directed to the left lobe after surgical exposure of the trachea. Mice were infected i.t. with 50 μL saline containing 1–5 × 10^6 CFU of serotype 19F *Spn* (Strain EF3030) or saline. Seven days later, only some mice were exposed again to Sp19F. Control mice received sterile saline on days 0 and 7. Lungs were collected and evaluated on day 0, 1, 3, 10, 14, 24 and 35 and processed for high-dimensional FSFC as previously described[20,21]. Data were analyzed using FlowJo v10.7 (BD Biosciences, Franklin Lakes, NJ, USA).

FTY720 Dosage

Experienced mice received 1mg/kg of FTY720 (Sigma-Aldrich, St. Louis, MO, USA) i.p. every other day for 12 days. Lungs were collected and processed for flow cytometry staining. Flow cytometry was performed on BD LSR II Flow Cytometer (BD Biosciences, Franklin Lakes, NJ, USA).

Intracellular staining for transcription factors

To evaluate transcription factor and nuclear factors, eBioscience Foxp3/Transcription Factor Staining Buffer Set (Thermo Fisher, Waltham, MA, USA) was used following manufacturer's protocols.

Ex vivo Stimulation and Intracellular cytokine staining

2×10^6 cells per 1×10^6 cells were blocked with TruStain αCD16/CD32 Fc-Block (Biolegend, San Diego, CA, USA) for 5 minutes before staining with optimized dilutions of mouse anti-CD69 (PE) and GL7 (APC) in FACS buffer for 35 min on ice. Cells were then washed and resuspended and plated in T cell media with 250 ng/mL of Phorbol Myristate Acetate (PMA) (LC Laboratories, Woburn, MA, USA), 1.5 ug/mL Ionomycin (Sigma-Aldrich, St. Louis, MO, USA), and Monensin (Biolegend, San Diego, CA, USA), and Brefeldin A (Biolegend, San Diego, CA, USA) for 6 hours at 37°C and 5% CO_2. Cells were then processed for ICS with Intracellular Fixation & Permeabilization Buffer Set (Thermo Fisher, Waltham, MA, USA) following manufacturer's instructions.

Flow cytometric assisted sorting (FACS)

Single-cell suspensions prepared from digested lungs were prepared with RBC lysis (Sigma-Aldrich, St. Louis, MO, USA) and blocked with TruStain αCD16/CD32 Fc-Block (BioLegend, San Diego, CA, USA) for 5 minutes. Cells were stained in FACS buffer with optimized dilutions of antibodies. $GL7^+$ and $GL7^-$ subsets of lung (i.v.$CD45.2^-$) $CD4^+$ T_{RM} cells were sorted into 20% FBS RPMI 1640 on ice with FACS-Aria II SORP (BD Biosciences, Franklin Lakes, NJ, USA). After sorting, cells were cultured for 6 hours with T cell media with or without PMA/Ionomycin stimulation at 37°C and 5% CO_2. Immediately after, cells were washed and pelleted into (RNA) ribonucleic acid Lysis Buffer (Qiagen, Germantown, MD, USA) and stored at −80°C until RNA extraction.

RNA Extraction and Quantitative Real-time PCR

RNA from sorted T cells was extracted using the RNAeasy Micro Kit (Qiagen, Germantown, MD, USA) following manufacturer's protocols and stored at −80°C. qRT-PCR was performed using the RNA-to-Ct kit (Thermo Fisher, Waltham, MA, USA). Primers for *Cmah* were commercially available TaqMan gene expression assays (Mm00483341_m1). We used 18s rRNA (Thermo Fisher, Waltham, MA, USA) to normalize expression levels of mRNA. Fold change of mRNA was calculated from all samples over unstimulated $GL7^-$ samples.

Duplex immunohistochemistry (IHC)

Mouse lung samples were embedded in optimal cutting temperature compound and subsequently sectioned at 5 μm using a CM3050 S cryostat (Leica, Wetzlar, Germany), with samples transferred to positively charged slides. Slides were allowed to air dry for 1 hour, before a 15-minute incubation in 10% neutral buffered formalin before progression to immunostaining. IHC was conducted using a Ventana Discovery Ultra (Roche, Basel, Switzerland), with detailed assay parameters outlined in Supplementary Table 2. Secondary (HRP) horse radish peroxidase conjugated species-specific antibodies were utilized to develop primary antibodies (Vector Laboratories, Burlingame, CA), with signal detection through TSA conjugated Opal fluorophores (Akoya Biosciences, Marlborough, MA, USA). Spectral (DAPI) 4′,6-diamidino-2-phenylindole was utilized to label nuclei (Akoya Biosciences, Marlborough, MA, USA). For figure preparation, 200x total magnification digitalized whole slide images of the duplex IHC assay were generated using a multispectral

Vectra Polaris Automated Quantitative Pathology Image System (Akoya Biosciences, Marlborough, MA, USA).

T cell Media

T cell media was prepared with RPMI 1640 (Thermo Fisher, Waltham, MA, USA) supplemented with 10% heat-inactivated fetal bovine serum, Penicillin/Streptomycin (100 U/mL, Thermo Fisher, Waltham, MA, USA), 1X Non-essential amino acids (Thermo Fisher, Waltham, MA, USA), 2 mM L-Glutamine (Glutamax, Thermo Fisher, Waltham, MA, USA), 1 nM Na-pyruvate (Thermo Fisher, Waltham, MA, USA), 10 mM HEPES (Thermo Fisher, Waltham, MA, USA) and 0.2 uM b-mercaptoethanol.

Calculation of relative multipotency index

We calculated the Relative Multipotency Index as previously described[21], using the following formula:

$$Relative Multipotency Index = \ln\left(\frac{\%of memory CD4 + T cells expressing \geq 2 LDTFs}{\%of memory CD4 + T cells expressing 1 LDTF}\right)$$

Statistical analyses

Statistical analyses were performed using Prism Version 9.2.0 (GraphPad, Boston, MA, USA). Differences were deemed statistically significant if the p value was ≤0.05. Each figure legend communicates the number of mice used, the experiment replicates performed, and the statistical tests used to make comparisons. For all figures, data are represented as mean ± (SEM) standard error of the mean.

Supplementary Material

Refer to Web version on PubMed Central for supplementary material.

FUNDING

This work was supported by NIH grants including K99 HL157555 to ATS, F31 HL142199 to KAB, F31 HL147397 to EIA, F30 HL158109 to NSE, F32 HL147461 to FTK, S10-OD026983 and SS10-OD030269 to NAC, RO1 HL136725 to MRJ, RO1 GM120060 and RO1 HL111449 to LJQ, RO1 AI115053, R35 HL135756, and R33 HL137081 to JPM and T32 HL007035 for support of trainees.

ACKNOWLEDGMENTS

The authors thank Boston University School of Medicine Flow Cytometry Core Facility (BU-FCCF) for their support of this project. We thank all the consenting donors for their generosity. We acknowledge the technical contributions of Aoife K. O'Connell and Hans P. Gertje in their histologic services provided through the NEIDL Comparative Pathology Laboratory (NCPL).

DATA AVAILABILITY

Data generated during and/or analyzed during the current study are available from the corresponding author on reasonable request.

REFERENCES

1. Torres A et al. Pneumonia. Nat. Rev. Dis. Primers 7, 25 (2021). [PubMed: 33833230]
2. Mizgerd JP Respiratory infection and the impact of pulmonary immunity on lung health and disease. Am. J. Respir. Crit. Care Med 186, 824–829 (2012). [PubMed: 22798317]
3. Quinton LJ & Mizgerd JP Dynamics of lung defense in pneumonia: resistance, resilience, and remodeling. Annu. Rev. Physiol 77, 407–430 (2015). [PubMed: 25148693]
4. Shenoy AT & Orihuela CJ Anatomical site-specific contributions of pneumococcal virulence determinants. Pneumonia (Nathan) 8, 7. [PubMed: 27635368]
5. Vardanjani HM, Borna H & Ahmadi A Effectiveness of pneumococcal conjugate vaccination against invasive pneumococcal disease among children with and those without HIV infection: a systematic review and meta-analysis. BMC Infect. Dis 19, 685 (2019). [PubMed: 31382917]
6. Wahl B et al. Burden of Streptococcus pneumoniae and Haemophilus influenzae type b disease in children in the era of conjugate vaccines: global, regional, and national estimates for 2000–15. Lancet Glob. Health 6, e744–e757 (2018). [PubMed: 29903376]
7. Hanquet G et al. Serotype replacement after introduction of 10-valent and 13-valent Pneumococcal conjugate vaccines in 10 countries, Europe. Emerg. Infect. Dis 28, 137–138 (2022). [PubMed: 34932457]
8. Weinberger DM, Malley R & Lipsitch M Serotype replacement in disease after pneumococcal vaccination. Lancet 378, 1962–1973 (2011). [PubMed: 21492929]
9. Malley R & Anderson PW Serotype-independent pneumococcal experimental vaccines that induce cellular as well as humoral immunity. Proc. Natl. Acad. Sci. U. S. A 109, 3623–3627 (2012). [PubMed: 22308483]
10. Smith NM et al. Regionally compartmentalized resident memory T cells mediate naturally acquired protection against pneumococcal pneumonia. Mucosal Immunol. 11, 220–235 (2018). [PubMed: 28513594]
11. Barker KA et al. Lung-resident memory B cells protect against bacterial pneumonia. J. Clin. Invest 131, e141810 (2021). [PubMed: 34060477]
12. Turner DL et al. Lung niches for the generation and maintenance of tissue-resident memory T cells. Mucosal Immunol. 7, 501–510 (2014). [PubMed: 24064670]
13. Masopust D & Soerens AG Tissue-resident T cells and other resident leukocytes. Annu. Rev. Immunol 37, 521–546 (2019). [PubMed: 30726153]
14. Teijaro JR et al. Cutting edge: tissue-retentive lung memory CD4 T cells mediate optimal protection to respiratory virus infection. J. Immunol 187, 5510–5514 (2011). [PubMed: 22058417]
15. McMaster SR, Wilson JJ, Wang H & Kohlmeier JE Airway-resident memory CD8 T cells provide antigen-specific protection against respiratory virus challenge through rapid IFN-γ production. J. Immunol 195, 203–209 (2015). [PubMed: 26026054]
16. Shenoy AT et al. Lung CD4+ resident memory T cells remodel epithelial responses to accelerate neutrophil recruitment during pneumonia. Mucosal Immunol. 13, 334–343 (2020). [PubMed: 31748706]
17. Son YM et al. Tissue-resident CD4+ T helper cells assist the development of protective respiratory B and CD8+ T cell memory responses. Sci. Immunol 6, eabb6852 (2021). [PubMed: 33419791]
18. Swarnalekha N et al. T resident helper cells promote humoral responses in the lung. Sci. Immunol 6:eabb6808. [PubMed: 33419790]
19. Kumar BV et al. Human tissue-resident memory T cells are defined by core transcriptional and functional signatures in lymphoid and mucosal sites. Cell Rep. 20, 2921–2934 (2017). [PubMed: 28930685]
20. Shenoy AT et al. CPHEN-011: Comprehensive phenotyping of murine lung resident lymphocytes after recovery from pneumococcal pneumonia. Cytometry A 101, 892–902 (2022). [PubMed: 34854229]
21. Shenoy AT et al. Antigen presentation by lung epithelial cells directs CD4+ TRM cell function and regulates barrier immunity. Nat. Commun 12, 5834 (2021). [PubMed: 34611166]

22. Naito Y et al. Germinal center marker GL7 probes activation-dependent repression of N-glycolylneuraminic acid, a sialic acid species involved in the negative modulation of B-cell activation. Mol. Cell Biol 27, 3008–3022 (2007). [PubMed: 17296732]
23. Belkina AC et al. Automated optimized parameters for T-distributed stochastic neighbor embedding improve visualization and analysis of large datasets. Nat. Commun 10, 5415 (2019). [PubMed: 31780669]
24. Sallusto F, Lenig D, Förster R, Lipp M & Lanzavecchia A Two subsets of memory T lymphocytes with distinct homing potentials and effector functions. Nature 401, 708–712 (1999). [PubMed: 10537110]
25. Seder RA & Ahmed R Similarities and differences in CD4+ and CD8+ effector and memory T cell generation. Nat. Immunol 4, 835–842 (2003). [PubMed: 12942084]
26. Laszlo G, Hathcock KS, Dickler HB & Hodes RJ Characterization of a novel cell-surface molecule expressed on subpopulations of activated T and B cells. J. Immunol 150, 5252–5262 (1993). [PubMed: 8515058]
27. Naito-Matsui Y et al. Functional evaluation of activation-dependent alterations in the sialoglycan composition of T cells. J. Biol. Chem 289, 1564–1579 (2014). [PubMed: 24297165]
28. Chen M et al. The development and function of follicular helper T cells in immune responses. Cell. Mol. Immunol 9, 375–379 (2012). [PubMed: 22659733]
29. Redelinghuys P et al. Early murine T-lymphocyte activation is accompanied by a switch from N-Glycolyl- to N-acetyl-neuraminic acid and generation of ligands for siglec-E. J. Biol. Chem 286, 34522–34532 (2011). [PubMed: 21835922]
30. Kerfoot SM et al. Germinal center B cell and T follicular helper cell development initiates in the interfollicular zone. Immunity 34, 947–960 (2011). [PubMed: 21636295]
31. Cyster JG & Schwab SR Sphingosine-1-phosphate and lymphocyte egress from lymphoid organs. Annu. Rev. Immunol 30, 69–94 (2012). [PubMed: 22149932]
32. Matloubian M et al. Lymphocyte egress from thymus and peripheral lymphoid organs is dependent on S1P receptor 1. Nature 427, 355–360 (2004). [PubMed: 14737169]
33. Wilk MM et al. Lung CD4 tissue-resident memory T cells mediate adaptive immunity induced by previous infection of mice with *Bordetella pertussis*. J. Immunol 199, 233–243 (2017). [PubMed: 28533445]
34. Lu YJ et al. Interleukin-17A mediates acquired immunity to pneumococcal colonization. PLoS Pathog. 4:e1000159.
35. Amezcua Vesely MC et al. Effector T_H17 cells give rise to long-lived T_{RM} cells that are essential for an immediate response against bacterial infection. Cell 178, 1176–1188.e15 (2019). [PubMed: 31442406]
36. Allie SR et al. The establishment of resident memory B cells in the lung requires local antigen encounter. Nat. Immunol 20, 97–108 (2019). [PubMed: 30510223]
37. Kinnear E et al. Airway T cells protect against RSV infection in the absence of antibody. Mucosal Immunol. 11, 249–256 (2018). [PubMed: 28537249]
38. Evans CM & Jenner RG Transcription factor interplay in T helper cell differentiation. Brief. Funct. Genomics 12, 499–511 (2013). [PubMed: 23878131]
39. Geginat J et al. Plasticity of human CD4 T cell subsets. Front. Immunol 5, 630 (2014). [PubMed: 25566245]
40. Oestreich KJ & Weinmann AS Master regulators or lineage-specifying? Changing views on CD4+ T cell transcription factors. Nat. Rev. Immunol 12, 799–804 (2012). [PubMed: 23059426]
41. Murasawa M et al. GL7 defines the cycling stage of pre-B cells in murine bone marrow. Eur. J. Immunol 32, 291–298 (2002). [PubMed: 11782020]
42. Harrison OJ et al. Commensal-specific T cell plasticity promotes rapid tissue adaptation to injury. Science 363:eaat6280. [PubMed: 30523076]
43. Quinton LJ, Walkey AJ & Mizgerd JP Integrative physiology of pneumonia. Physiol. Rev 98, 1417–1464 (2018). [PubMed: 29767563]
44. Curtis MM & Way SS Interleukin-17 in host defence against bacterial, mycobacterial and fungal pathogens. Immunology 126, 177–185 (2009). [PubMed: 19125888]

45. Arafa EI et al. Recruitment and training of alveolar macrophages after pneumococcal pneumonia. JCI Insight 7:e150239.

46. Karo-Atar D et al. A protective role for IL-13 receptor α 1 in bleomycin-induced pulmonary injury and repair. Mucosal Immunol. 9, 240–253 (2016). [PubMed: 26153764]

47. Macauley MS et al. Unmasking of CD22 co-receptor on germinal center B-cells occurs by alternative mechanisms in mouse and Man. J. Biol. Chem 290, 30066–30077 (2015). [PubMed: 26507663]

48. Peri S, Kulkarni A, Feyertag F, Berninsone PM & Alvarez-Ponce D Phylogenetic distribution of CMP-Neu5Ac hydroxylase (CMAH), the enzyme synthetizing the proinflammatory human xenoantigen Neu5Gc. Genome Biol. Evol 10, 207–219 (2018). [PubMed: 29206915]

49. Jellusova J & Nitschke L Regulation of B cell functions by the sialic acid-binding receptors siglec-G and CD22. Front. Immunol 2, 96 (2012). [PubMed: 22566885]

50. Nitschke L, Carsetti R, Ocker B, Köhler G & Lamers MC CD22 is a negative regulator of B-cell receptor signalling. Curr. Biol 7, 133–143 (1997). [PubMed: 9016707]

51. Garcia S, DiSanto J & Stockinger B Following the development of a CD4 T cell response in vivo: from activation to memory formation. Immunity 11, 163–171 (1999). [PubMed: 10485651]

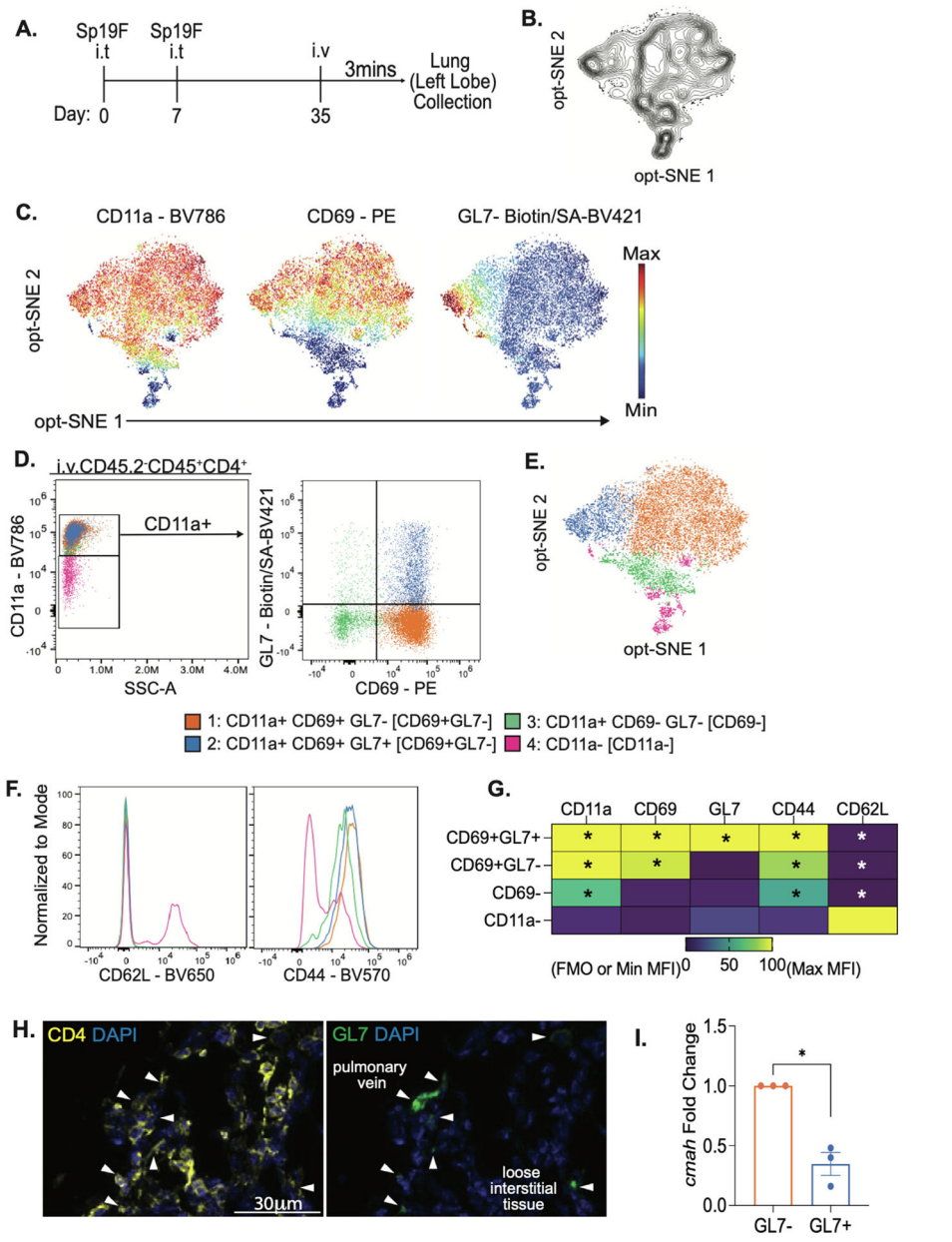

Fig. 1.

Lungs from pneumococcus-experienced mice contain multiple subsets of memory $CD4^+$ T cells. (A) Model of heterotypic immunity. Adult female mice are infected intratracheally into the left lobe (LL) of the lungs with *Streptococcus pneumoniae* serotype 19F (Sp19F) on day 0 and 7 then rested until day 35, referred to as experienced. Three minutes before LL collection, mice were injected Intravenously. with mouse anti-CD45.2 antibody then processed for flow cytometry. (B) Optimized parameter T-distributed stochastic neighborhood embedding (opt-SNE) visualization depicting live lung ($ivCD45.2^-$) $CD45^+CD3^+CD4^+$ T cells of concatenated data from $n = 6$ mice gathered over two independent experiments. (C) Heat map depiction of expression level of surface markers overlayed on opt-SNE map. (D) Representative manual gating of flow cytometry data of

lung $CD4^+$ T cells, $n = 6$ mice, two independent experiments**. (**E) Manual gates overlayed on opt-SNE map.(F) Representative histograms of CD62L and CD44 in lung $CD4^+$ T cells, $n = 6$, 2 independent experiments. (G) Heatmap of average mean fluorescence intensity (MFI) normalized to fluorescence minus one (FMO) controls or minimal MFI and maximal MFI, $n = 6$, two independent experiments. Each group was compared to $CD11a^-$ for statistical comparisons, one-way ANOVA $*p < 0.002$. (H) Representative immunofluorescent micrograph showing anatomical distribution of $CD4^+$ (yellow) and $GL7^{+6}$ cells in experienced mouse lungs at 35 dpi, with white arrows indicating some double-positive cells. (I) Fold change of *Cmah* mRNA in $GL7^+$ over $GL7^-$ sorted, unstimulated, lung $CD4^+CD11a^+CD69^+$ T cells, $n = 3$, 6 LL pooled per sample, Welch's T-test, *p value = 0.0210.

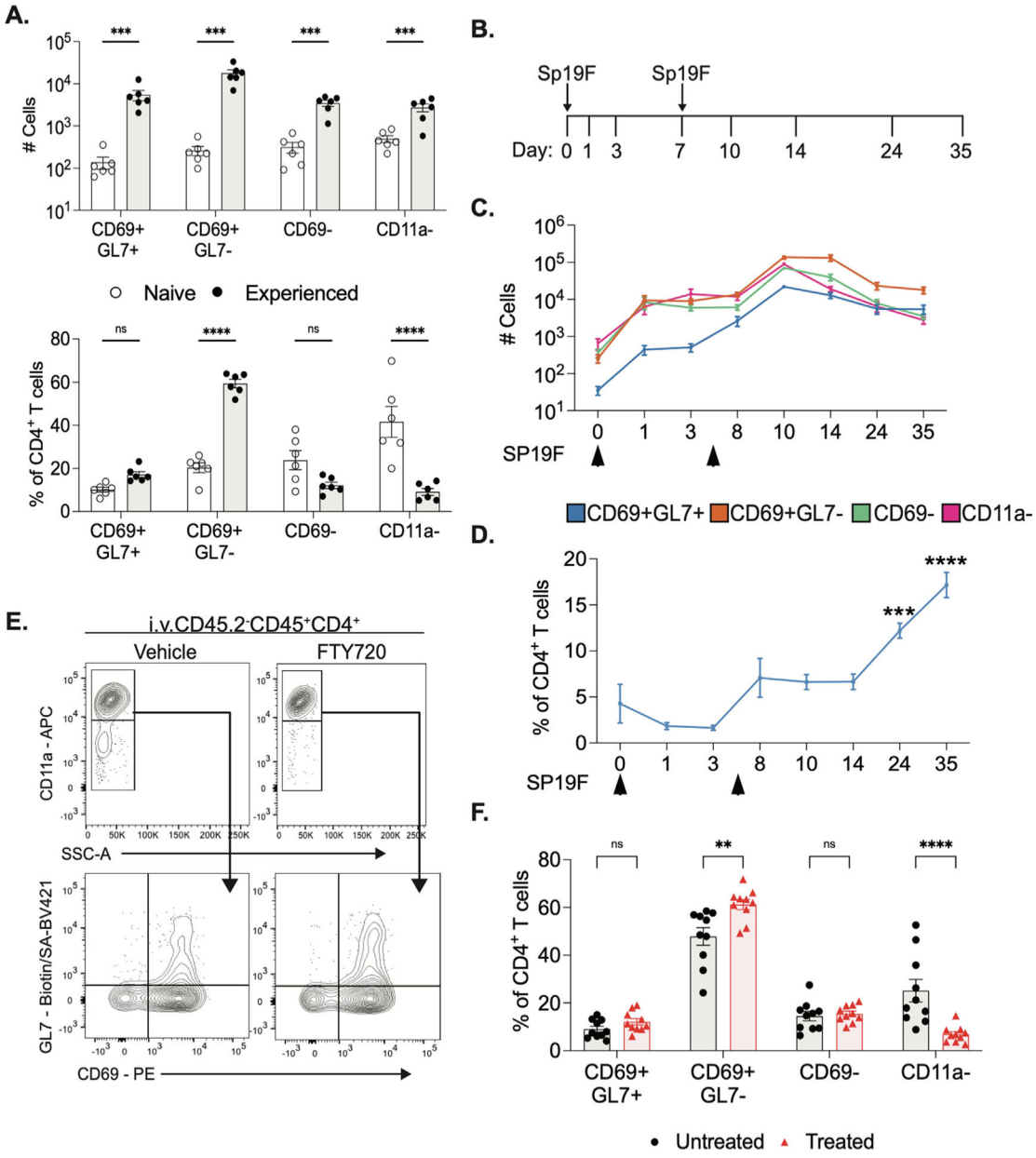

Fig. 2.

$CD69^+GL7^+$ subsets of $CD4^+$ T cells have distinct dynamic patterns of accumulation in mouse lungs. (A) Numbers of cells (above) and percentage of lung $CD4^+$ T cells in LL (below) of each subset from saline or Spn experienced mice at 35dpi, $n = 6$, two independent experiments. Bar graphs of mean and error bars of standard error of mean[5], 2-way ANOVA with Bonferroni multiple comparisons test, ***$p < 0.0003$, ****$p < 0.0001$. (B) Diagram of timeline of lung collection. Sp19F intratracheally. on days 0 and 7. (C) Average number of cells in LL at every collection timepoint, $n = 6$ per timepoint, 2 independent experiments, error bars are SEM. (D) Average percent of $CD4^+$ T cells in LL from $CD69^+GL7^+$ subset, $n = 6$ per timepoint, two independent experiments, error bars are SEM. One-way ANOVA with Bonferroni multiple comparisons test, ***$p = 0.0004$ ****$p < 0.0001$. FTY720 or

vehicle Intraperitonealy to experienced mice at 1mg/kg every other day for 12 days. (E) Representative flow cytometry plots of lung $CD4^+$T cells from LL, $n = 10$ per group, two independent experiments. (F) Quantification of percent of $CD4^+$ T cells in LL, error bars are SEM. Two-way ANOVA with Bonferroni multiple comparisons test, $^{**}p = 0.0013$ $^{****}p < 0.0001$.

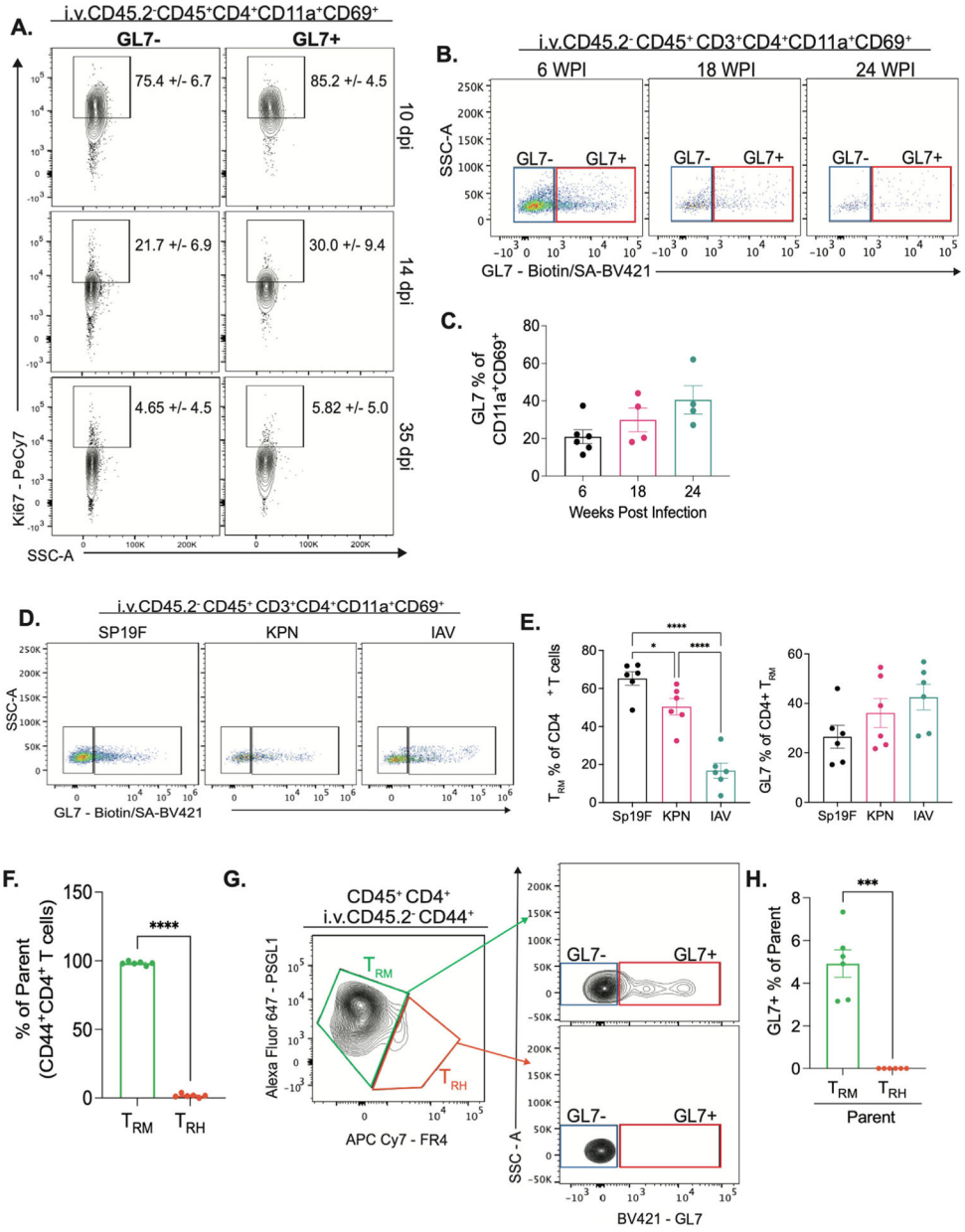

Fig. 3.

CD69+GL7+ subsets of CD4+ T cells have characteristics of resident memory T cells. (A) Flow cytometry of single cell suspensions from LL collected at 10, 14 and 35dpi. Representative plots of Ki67 staining in $GL7^+$ or $GL7^-$ of $CD69^+CD11a^+$ $CD4^+$ T cells in LL. Mean +/− standard deviation of percent of parent, $n = 5$ to 6 per dpi, two independent experiments. LL of Sp19F experienced mice collected at 6, 18 and 24 wpi. (B) Representative flow cytometry plots of GL7 staining, $n = 4$ to 6 per group, two independent experiments. (C) Quantification of percent of $GL7^+$ o of $CD69^+CD11a^+$ $CD4^+$ T cells in LL, error bars are SEM, ordinary one-way ANOVA with Tukey multiple comparisons test. Mice infected intratracheally to the LL with SP19F, killed Klebsiella pneumoniae or Influenza A/PR8 on day 0 and 7 and rested until day 40. LL collected for flow cytometry.

(D) Representative flow cytometry plots of GL7 staining, $n = 6$ per group, two independent experiments. (E) , Quantification of percent of T_{RM} cells of $CD4^+$ T cells (right) and percent of $GL7^+$ in $CD4^+$ T_{RM} cells in LL of each infection model, error bars are SEM, ordinary one-way ANOVA with Tukey multiple comparisons test, $*p = 0.0464$, $****p < 0.0001$. LL from Sp19 experienced mice processed with manual digestion method after anti-ARTC2 nanobody Intravenous injection for 30min. (F) Quantification of percent of T_{RH} and T_{RM} cells of parent ($CD44^+CD4^+$ T cells), error bars are SEM, paired T-test, $****p < 0.0001$. (G) Representative flow cytometry plots of of T_{RH} and T_{RM} cells (right) and GL7 staining (left) of parent population, $n = 6$, two independent experiments. (H) Quantification of percent of $GL7^+$ percent of parent (T_{RM} or T_{RH}), error bars are SEM, paired T-test, $**p = 0.0015$.

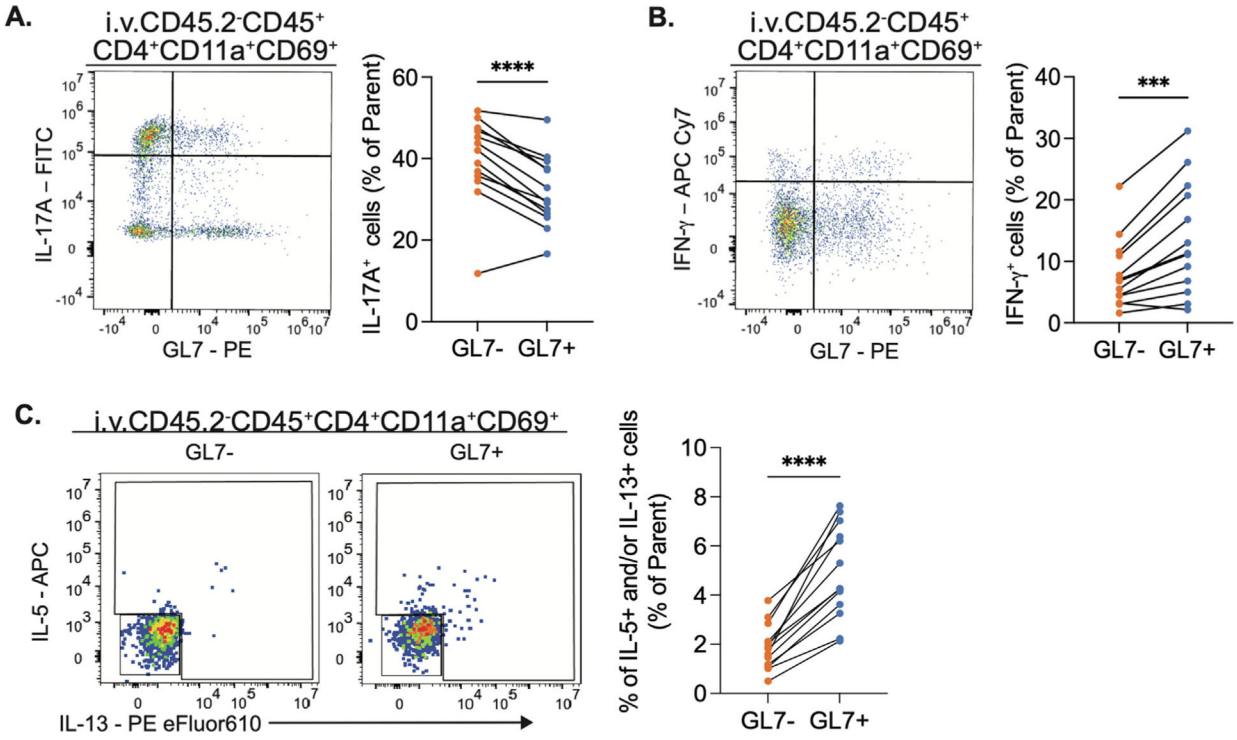

Fig. 4.

GL7$^+$ T_{RM} cells secrete similar cytokines reflective of their transcription factor profiles. Intracellular cytokine staining (ICS) of lung (Intravenous injection CD45.2$^-$) CD4$^+$$T_{RM}$ cells stimulated *ex vivo* with PMA/Ionomycin in presence of golgi plug and golgi block. (A) Representative plot of IL-17A (right) and quantification of frequency of IL-17A$^+$ cells (left) in parent population (GL7$^+$ or GL7$^-$ CD4$^+$$T_{RM}$ cells). (B) Representative plot of IFN-γ (right) and quantification of frequency of IFN-γ$^+$ cells (left) in parent population (GL7$^+$ or GL7$^-$ CD4$^+$$T_{RM}$cells). (C) Representative plots of IL-5/IL-13 (right) and quantification of percent of IL-13$^+$ and/or IL-5$^+$ cells in parent population (GL7$^+$ or GL7$^-$ CD4$^+$$T_{RM}$ cells). Paired t test, ***$p = 0.0002$, ****$p < 0.0001$. $n = 13$, two independent experiments.

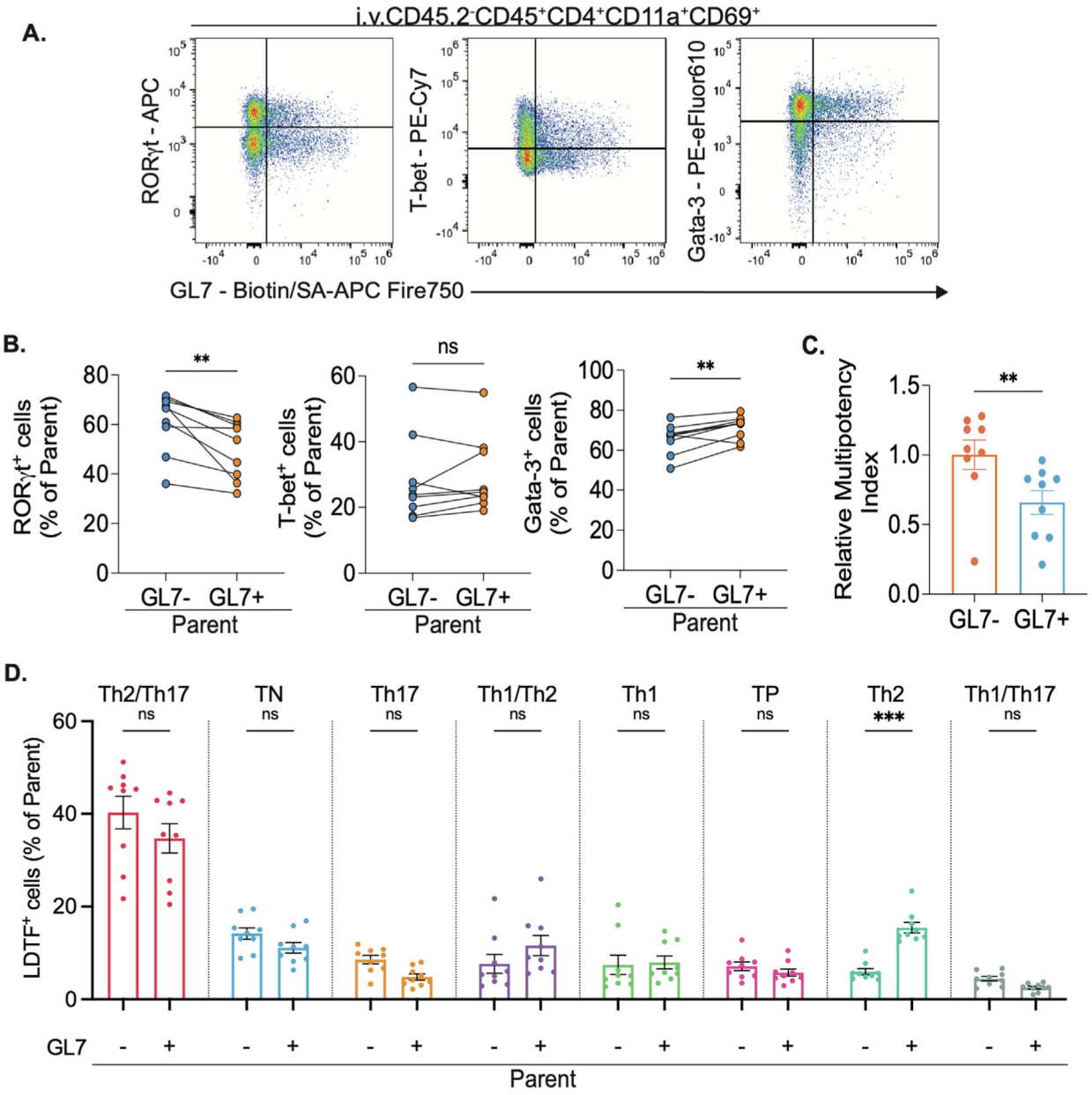

Fig. 5.

GL7$^+$ T_{RM} cells have unique transcription factor profiles. (A) Representative flow cytometry plots of intracellular lineage-defining transcription factor (LDTF) staining in live lung CD4$^+$$T_{RM}$ cells and (B) Frequency of LDTF$^+$ cells in parent population (GL7$^+$ and GL7$^-$ CD4$^+$$T_{RM}$). Paired t test, $^{**}p = 0.005$. (C) Relative multipotency index[21] of GL7$^+$ and GL7$^-$ lung (Intravenous injection CD45.2$^-$) CD4$^+$$T_{RM}$ cells. Bar graphs of mean and error bars of SEM. Ratio paired t test, $^{**}p = 0.0044$. $n = 9$, two independent experiments. (D) Frequency of GL7$^+$ or GL7$^-$ CD4$^+$$T_{RM}$ from each lineage in parent population (GL7$^+$ and GL7$^-$ CD4$^+$$T_{RM}$). Bar graph of mean and error bars of SEM. Two-way ANOVA with Bonferroni multiple comparisons test, $^{***}p = 0.0008$

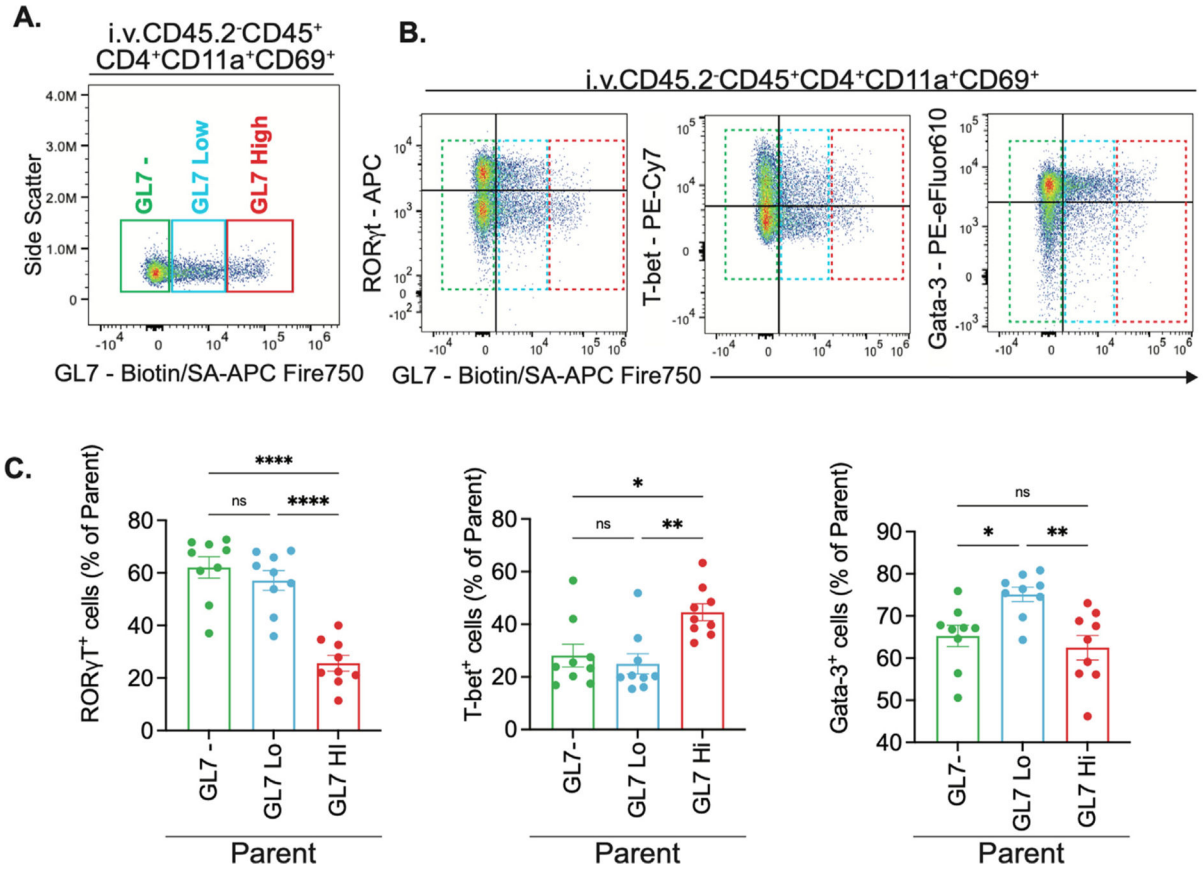

Fig. 6.

GL7^{+} T_{RM} cells are a bimodal population with different roles. (A) Manual gating of GL7^{-}, GL7^{Low} and GL7^{High} in lung (Intravenous injection CD45.2^{-}) CD4^{+}T_{RM} cells. (B) Representative flow cytometry plots of intracellular LDTF staining in lung (Intravenous injection CD45.2^{-}) CD4^{+}T_{RM} with GL7^{-}, GL7^{Low} and GL7^{High} gates. (C) Frequency of RORγT^{+}, T-bet^{+} and Gata-3^{+} cells in parent population (GL7^{-}, GL7^{Low} and GL7^{High}CD4^{+}T_{RM}). Bar graphs of mean and error bars of SEM. One-way ANOVA with Tukey test of multiple comparisons. *$p = 0.02$, **$p = 0.003$, ****$p < 0.0001$. $n = 9$, two independent experiments.